American Mineralogist, Volume 94, pages 156–165, 2009

Structural position of H_2O molecules and hydrogen bonding in anomalous 11 Å tobermorite

SERGEY V. CHURAKOV*

Paul Scherrer Institute, CH-5232 Villigen PSI, Switzerland

ABSTRACT

For the first time, the structure and dynamics of H_2O in the interlayer of anomalous 11 Å tobermorite have been analyzed based on ab initio molecular dynamics simulations. The simulations provide detailed information on the structure of the hydrogen bonds formed by H_2O molecules and OH groups. The calculated structural parameters of the tobermorite building blocks are in good agreement with the experimental model of Merlino et al. (1999), which is based on X-ray diffraction (XRD) measurements. However, in contrast to the measurements, the simulations suggest that the W1 and W3 sites are split between two general positions with 50% occupancy. It is proposed that the experimental studies provide only averaged coordinates of these sites due to the limitations imposed by the polytypic structures. Analysis of the H_2O dynamics at 321 and 506 K suggest the possibility of a temperature induced order-disorder transition associated with the orientation of O6H···W1 and O6H···W3 hydrogen bonds in the structure of anomalous 11 Å tobermorite. The experimental IR and Raman spectra of 11 Å tobermorite are interpreted based on analyses of the vibrational density of states.

Keywords: Tobermorite, C-S-H phases, water, molecular dynamics

INTRODUCTION

The mineral group tobermorite comprises several layered calcium silicate hydrates (C-S-H) with common structural modules, different degrees of hydration, and variable compositions of the interlayer (Bonaccorsi et al. 2005; Merlino et al. 1999). The natural samples are found in hydrothermally altered carbonate rocks and vesicle fillings of basalts. The crystallographic model of tobermorite is used as a basic structural concept for amorphous C-S-H, which is the main phase of ordinary Portland cement (Cong and Kirkpatrick 1996; Kirkpatrick et al. 1997; Richardson 2004; Taylor 1997). Furthermore, the formation of crystalline tobermorite phases is expected in the cement used in deep geological repositories for radioactive waste (Jantzen 1984). Similar to zeolites, the structure of tobermorite has cavities that can incorporate H_2O and various ionic species (Richardson 2004). A detailed knowledge of tobermorite chemistry is therefore indispensable for understanding the chemical, structural, and technological properties of cement compounds and their derivatives and for the development of new materials.

The first structural model for tobermorite was proposed by Megaw and Kelsey (1956). According to the most recent crystal-structure refinements (Bonaccorsi et al. 2005; Merlino et al. 1999, 2001), the basic structural module of tobermorite is formed by a layer of seven-coordinated Ca atoms. Wollastonite type chains of silicate tetrahedra, running along the *b* axis, are attached to both sides of the Ca layer (Fig. 1). The silicate tetrahedra may occupy two alternative positions displaced by a translation vector of length *b*/2. Due to variations in the structural position of the tetrahedral chain, the natural samples usually show long-range stacking disorder. Depending on the degree of hydration and the composition of the interlayer, some neighboring Ca layers are connected through bridging interlayer cations and bridging tetrahedral sites, and others directly by a single silicate chain. The interlayer space may be occupied by various cations and H_2O.

Three tobermorite phases have been differentiated on the basis of their basal spacing: 14 Å tobermorite [plombierite, $Ca_5Si_6O_{16}(OH)_2{\cdot}7H_2O$], 11 Å tobermorite with a variable composition in the interlayer [$Ca_{5-x}Si_6O_{17-2x}(OH)_{2x}{\cdot}5H_2O$] and H_2O-free 9 Å tobermorite [$Ca_5Si_6O_{16}(OH)_2$, riversideite]. Upon heating to about 353–373 K the 14 Å tobermorite transforms into the 11 Å tobermorite. Calcium-rich 11 Å tobermorite (the so called "normal" form) loses its interlayer H_2O at 573 K and further transforms to the 9 Å tobermorite. In contrast, the "anomalous" 11 Å tobermorite [a Ca-poor polymorph with the chemical composition $Ca_4Si_6O_{15}(OH)_2{\cdot}5H_2O$] does not collapse to the 9 Å tobermorite upon dehydration. Variations in the thermal behavior of 11 Å tobermorite were initially explained by different relative arrangements of the tetrahedral chains in the "normal" and "anomalous" forms (Wieker et al. 1982). However, it was recently shown that both "normal" and "anomalous" tobermorite forms have the identical arrangement of tetrahedral chains (Merlino et al. 1999, 2001). Alternatively, the difference in the thermal behavior was explained by the presence of interlayer Ca ions in the normal tobermorite, which requires the collapse of the building blocks to compensate for the loss of H_2O molecules in the coordination shell of interlayer Ca upon dehydration (Merlino et al. 1999, 2001).

The crystal structure and the order-disorder character of 11 Å tobermorite (normal and anomalous forms) have been successfully studied using X-ray diffraction (XRD) (Merlino et al. 1999, 2001). The studies report the structure of the Ca layer, the relative orientation of the silicate chains, and the refined positions of H_2O and Ca ions in the interlayer. Since the position of hydro-

* E-mail: sergey.churakov@psi.ch

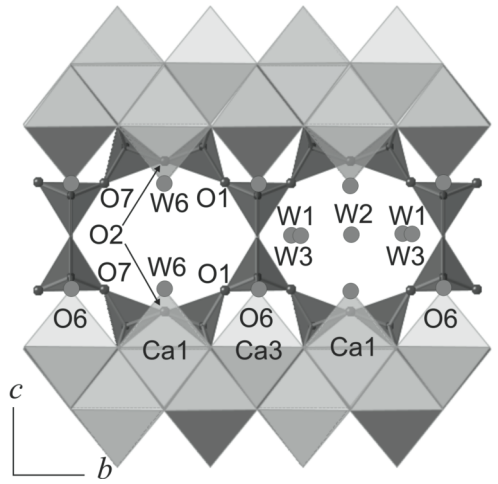

FIGURE 1. Crystal structure and distribution of H_2O sites in the anomalous form of 11 Å tobermorite as proposed by Merlino et al. (2001). The H_2O sites (W1, W2, W3, and W6), OH groups (O6), and O atoms relevant for the hydrogen bonding (O1, O2, and O7) are indicated. Calcium and silicon sites are shown as rendered polyhedra. See Table 2 for the experimental and the theoretical coordinates.

gen atoms cannot be resolved by XRD techniques, the detailed structural role of H_2O remains unknown. Molecular modeling is an appropriate tool to obtain complementary information on the structure and dynamics of hydrous species in mineral phases on an atomic scale. Atomistic simulations of C-S-H phases are still rare, due to the high complexity of the system. Nonetheless, there is growing interest in the application of molecular modeling in the field of cement chemistry. Recently, the structure of the water at the tobermorite interface was studied by molecular dynamics (MD) using an empirical force field (Kalinichev and Kirkpatrick 2002; Kalinichev et al. 2007). The preferential position of Al impurities in the silicate chain of tobermorite was studied using ab initio, semi-empirical molecular orbital calculations and force field methods (Faucon et al. 1997, 1999; Kashihara et al. 1994). Several studies have focused on the structural and mechanical properties of other C-S-H phases (Bell and Coveney 1998; Churakov and Mandaliev 2007; Coveney and Humphries 1996; Gmira et al. 2004; Kirkpatrick et al. 2005).

In this work, quantum mechanical calculations based on the density functional theory (DFT) have been performed to reveal the structural positions and dynamics of H_2O in the anomalous 11 Å tobermorite. In contrast to classical simulations based on empirical force fields, quantum mechanical calculations do not require a preliminary calibration of interaction parameters for the system of interest. Thus, the "parameter free" ab initio methods are particularly beneficial for studying complex C-S-H phases. However, it should be kept in mind that ab initio methods use several approximations that may have an effect on the results and efficiency of simulations (Goedecker 1999; Payne et al. 1992). The accuracy of such approximations should usually be assessed by benchmarking against well-characterized systems. The practical application of ab initio methods is limited to systems of small size (up to several hundreds atoms) and short simulation times of several tens of picoseconds due to their high computational costs. Thus, the system of interest must be simplified for the sake of efficiency. The anomalous form of 11 Å tobermorite [MDO_2 polytype (Merlino et al. 2001)] was considered as being one of the simplest phases in the tobermorite group that also contains interlayer H_2O. Since the anomalous 11 Å tobermorite does not contain interlayer cations, the study is focused exclusively on the role of H_2O in the interlayer of tobermorite. Possible variations in tobermorite chemistry, including dehydration, defects in the tetrahedral chain and isomorphic substitutions remain, therefore, beyond the scope of this study. A further purpose of this study was to test the performance of the linear-scaling methods (Goedecker 1999) recently implemented in the CP2K package (VandeVondele et al. 2005) against the common plane wave techniques (CPMD 1997–2001). The former method seems to be more efficient in the case of large systems and long simulation times. Furthermore, the Born-Oppenheimer MD approach used in CP2K simulations overcomes some technical difficulties of Car-Parrinello MD (see following section for details) recently noticed in the simulation of bulk water (Kuo et al. 2006). The structural properties of 11 Å tobermorite obtained with the CP2K package are compared with the equivalent calculations performed with the "traditional" density functional methods using a plane wave basis set (CPMD 1997–2001). This study is considered to be a first step toward the comprehensive ab initio modeling of other tobermorite forms and amorphous C-S-H phases.

METHOD AND SIMULATION SETUP

CP2K simulations

Ab initio MD simulations of 11 Å tobermorite were performed based on the density functional theory (Hohenberg and Kohn 1964; Kohn and Sham 1965) implemented in the QUICKSTEP/CP2K simulation package (VandeVondele et al. 2005) using the Gaussian and Plane Wave method (GPW) (Lippert et al. 1997). In the GPW method, the Kohn-Sham orbitals are expanded using a linear combination of atom-centered Gaussian type orbital functions. The electron charge density is expanded using an auxiliary basis set of plane waves (PW) up to a 320 Ry cutoff. The PBE exchange and correlation functional (Perdew et al. 1996) used in this work is known to accurately reproduce the structural properties of water (Grossman et al. 2004). The dual space norm-conserving pseudopotentials of Goedecker et al. (1996) were applied to avoid explicit consideration of core electrons. Triple-ζ valence basis sets, augmented with two sets of polarization functions optimized for use with the selected pseudopotentials, were employed for O and H using $2s^2 2p^4$ and $1s^1$ valence configurations, respectively. For Ca and Si, double-ζ valence basis sets, augmented with d-type polarization functions, were applied, employing $3s^2 3p^4 4s^2$ and $3s^2 3p^2$ states in the valence shell, respectively.

Accuracy of the basis sets, pseudopotentials and the other simulation parameters were tested against geometries of simple molecules of H, O, Si, and Ca in gas phase as well as the lattice constants of Ca and Si oxides. The calculations reproduce the experimental geometries within 1.0%. The lattice parameters of oxides were reproduced within 1.5%. It is worth mentioning that a similar simulation setup, except for the BLYP exchange and correlation functional (Becke 1988; Lee et al. 1988), has been already used successfully in the simulations of bulk water (Kuo et al. 2004).

Ab initio MD simulations based on the Born-Oppenheimer approximation were performed with a time step of 1.0 fs. Before every force evaluation step, the energy was converged to within 3×10^{-10} au/atom using a single k-point in the origin of the Brillouin zone (Γ-point sampling). The simulations were started from the crystal-structure model proposed by Merlino et al. (2001) for anomalous 11 Å tobermorite. Since the experimental model does not provide the positions of hydrogen atoms, the H_2O molecules were initialized with an arbitrary orientation, centered in the oxygen sites. The system was equilibrated for at least 20 ps. The initial 5 ps of equilibration were conducted at 400 K to speed up the rearrangement of water molecules in the interlayer followed by annealing to the target temperature. The structural parameters of tobermorite and the H_2O dynamics were deduced from a 20 ps production run in a microcanonical ensemble at an average temperature T = 321 K. A supplementary molecular dynamics trajectory (20 ps production

run) was performed at 506 K to speed up the reorientation dynamics of hydrogen bonds and to assess the effect of thermal disorder on the structural position of H_2O molecules in the interlayer.

Supercell setup for CP2K simulations

The implementation of the DFT methods in the CP2K package is limited to the orthorhombic simulation cell. The structure of the MDO_2 polytype of 11 Å tobermorite was solved in the monoclinic space group $B11m$. Taking into account that the γ angle (123.18°) is close to the ideal value of 120° and the symmetry of the building blocks in tobermorite has the orthorhombic layer group symmetry $C2m(m)$, the unit cell can be transformed to the orthogonal supercell by doubling the lattice parameters in the "a" direction (see also Fig. 3 in Merlino et al. 2001). The parameters of the simulation supercell, and the simulation conditions, are summarized in Table 1.

CPMD simulations

Since the CP2K code has not been widely used for the modeling of mineral phases before, additional test calculations on anomalous 11 Å tobermorite were performed with the plane wave DFT method (CPMD 1997–2001) using the experimental geometry of the supercell (Table 1). The simulations were performed using the BLYP exchange and correlation functional (Becke 1988; Lee et al. 1988) and Troullier-Martins pseudopotentials (Troullier and Martins 1991). The $3s^23p^2$ states of silicon, $2s^22p^4$ states of oxygen, $1s^1$ states of hydrogen, and $3s^23p^44s^2$ states of calcium were included in the valence and expanded in a plane wave basis set up to a 70 Ry cutoff. The Car-Parrinello MD simulations (Car and Parrinello 1985) were performed in the NVT ensemble using 0.12 fs time steps and a fictitious electron mass set at 900 au. The temperature (Table 1) was controlled using a Nose-Hoover chain of thermostats (Hoover 1985; Nose 1984). The H atoms were modeled using the mass of deuterium to allow for longer integration time steps. The system was equilibrated for 5 ps starting from a similar configuration used in the CP2K run. The geometric parameters were obtained by averaging over about 8 ps of the production run. The accuracy of the pseudopotentials, and PW expansion were tested against geometries of simple molecules of H, O, Si, and Ca in the gas phase as well as the lattice constants of Ca and Si oxides. Exactly the same set of simulation parameters was recently used to study the structure of the crystalline calcium silicate hydrate-xonotlite (Churakov and Mandaliev 2007).

The total MD trajectory generated with the CPMD code is almost three times shorter than the one provided by the CP2K simulations. The CMPD results are only used to prove the capability of CP2K simulations to reproduce the basic structural elements of tobermorite building blocks. The dynamics and structure of interlayer sites are deduced from the long CP2K trajectories. Thus a comparison between the results obtained with CP2K and CPMD packages enabled us to test the effects of supercell geometry and performance of the localized basis set vs. plane waves for C-S-H phases.

Born-Oppenheimer approach vs. Car-Parrinello MD

In the Car-Parrinello MD approach, the electronic degrees of freedom are treated classically via the introduction of a fictitious electronic kinetic energy term in the extended Lagrangian of the system (Car and Parrinello 1985). The fictitious mass of electronic wavefunctions is chosen in such a way as to enable the efficient integration of the equations of motion and guarantee an adiabatic separation of nuclear and electronic degrees of freedom (Blöchl and Parrinello 1992). It has been shown, however, that some degree of nonadiabaticity exists for any value of the fictitious electronic mass (Tangney 2006; Tangney and Scandolo 2002). Thus, heat is inevitably transferred from nuclei to electrons resulting in a decrease of the ionic temperature during simulations. It was suggested therefore to use the Nose-Hoover chain of thermostats for long Car-Parrinello MD simulations (Kuo et al. 2004). Instead, in the Born-Oppenheimer approach, the wave functions are quenched to the ground state before each step of interatomic force calculations (Payne et al. 1992). The accuracy and time-reversibility of the ionic trajectory depends strongly on the convergence of the wave functions. A critical inspection of the Car-Parrinello and Born-Oppenheimer results for bulk water has shown that the structural properties predicted by both methods are similar if the fictitious electronic mass in the Car-Parrinello simulations is taken to be reasonably small and/or a thermostat method is used (Grossman et al. 2004; Kuo et al. 2004; Schwegler et al. 2004). However, the presence of a fictitious electronic mass parameter in Car-Parrinello dynamics inevitably shifts vibrational power spectra in the region of lower frequencies (Kuo et al. 2006). The simulation setup for the Car-Parrinello simulations used in this work is consistent with the recommended values of fictitious electron mass and use of the thermostats (Grossman et al. 2004; Kuo et al. 2004). Thus, we expect agreement of the average structural properties of tobermorite obtained from Car-Parrinello and Born-Oppenheimer molecular dynamics. The vibrational power spectra obtained from the Car-Parrinello simulation must be extrapolated to the limit of an infinitely small fictitious mass of electrons (Kuo et al. 2006).

Table 1. Parameters of the supercell used in the simulation of anomalous 11 Å tobermorite, duration of equilibration/production runs (Eql/Prod), and the average simulation temperature

	a	*b*	*c* (Å)	Eql/Prod (ps)	*T* (K)
	α	β	γ (°)		
CPMD	13.47	14.74	22.487	5/8	300
	90	90	123.25		
CP2K	11.265	14.792	22.487	20/20	321
	90	90	90	5/20	506

Hydrogen bond dynamics

The dynamics of hydrogen bonds formed by H_2O molecules was analyzed based on the correlation function of the hydrogen bond population. The hydrogen bond "continuous" lifetime correlation function (Rapaport 1983) is defined as:

$$C_{ij}(t) = \frac{\left\langle h_{ij}(\tau) H_{ij}(\tau + t) \right\rangle}{\left\langle h_{ij}(\tau) \right\rangle} \quad (1)$$

where $h_{ij}(\tau)$ is the population variable, which is unity when a particular hydrogen site i donates a hydrogen bond to an O site j at time τ, and is zero otherwise. Furthermore, $H_{ij}(\tau + t) = 1$ if a target ij pair remains continuously hydrogen bonded during the time t, and is zero otherwise. A simple geometric criterion has been used to define hydrogen bonds, e.g., the bond is considered to be formed if the distance between O and H sites is shorter than 2.4 Å (Kalinichev and Churakov 2001). For the exponential decaying correlation function, the relaxation time constant $\tilde{\tau}_{ij}$ is a measure of the bond lifetime (Chandler 1987):

$$C_{ij}(t) \sim e^{-\frac{t}{\tilde{\tau}_{ij}}}. \quad (2)$$

Vibrational density of states in the tobermorite was calculated by Fourier transform of the velocity autocorrelation function (Allen and Tildesley 1987) using the maximum entropy method (Press et al. 1992). To compare the CPMD results with the CP2K calculations and the experimental data, the spectral lines of deuterium had to be corrected for isotopic substitution and the "fictitious mass" of electrons in the Car-Parrinello molecular dynamics. In a harmonic approximation, the frequency shift due to substitution of hydrogen by deuterium can be expressed by

$$\nu_H = \nu_D \sqrt{\frac{M_D}{M_H}} \approx \nu_D \sqrt{2} \quad (3)$$

where ν_H/M_H and ν_D/M_D are vibrational frequencies and masses of hydrogen and deuterium, respectively. The scaling parameter ($\alpha = 1.04$) was used to extrapolate the vibrational frequencies in the mid-infrared region to the limit of an infinitely small fictitious mass (Tangney 2006; Tangney and Scandolo 2002).

Results

Structural parameters of tobermorite: Comparison of theoretical and experimental data

Atomic coordinates of anomalous 11 Å tobermorite obtained from the CP2K and the CPMD trajectories are compared with the experimental data (Merlino et al. 2001) in Table 2. Both CPMD and CP2K simulations show good overall agreement with the experimental results for the Ca, Si, and non-aqueous O sites. The positions of O6 and H_2O sites are also in reasonable agreement with the experimental data, although they show larger deviations. Although, the CPMD and CP2K simulations were

TABLE 2. Atomic coordinates obtained from ab initio simulation using CPMD and CP2K packages compared with the experimental data of Merlino et al. (2001)

	This Work									Experimental		
	CP2K (321 K)			CP2K (506 K)			CPMD (300 K)			Merlino et al. (2001)		
	x	y	z	x	y	z	x	y	z	x	y	z
Ca1	0.265	0.433	0.204	0.264	0.433	0.204	0.266	0.434	0.204	0.2651	0.4328	0.2056
Ca3	0.750	0.923	0.294	0.751	0.923	0.294	0.750	0.924	0.293	0.7499	0.9228	0.2935
Si1	0.755	0.386	0.158	0.755	0.387	0.158	0.757	0.389	0.158	0.7581	0.3862	0.1574
Si2	0.911	0.755	0.071	0.913	0.756	0.071	0.917	0.759	0.071	0.9087	0.7531	0.0712
Si3	0.757	0.970	0.157	0.757	0.969	0.157	0.759	0.971	0.157	0.7592	0.9697	0.1577
O1	0.767	0.507	0.094	0.769	0.507	0.093	0.776	0.512	0.094	0.7710	0.5059	0.0942
O2	0.753	0.176	0.130	0.751	0.175	0.131	0.759	0.181	0.132	0.7590	0.1780	0.1327
O3	0.988	0.540	0.200	0.986	0.540	0.199	0.985	0.541	0.200	0.9850	0.5369	0.1982
O4	0.514	0.305	0.195	0.513	0.306	0.194	0.515	0.307	0.193	0.5190	0.3063	0.1942
O5	0.399	0.748	0.506	0.402	0.749	0.500	0.408	0.753	0.501	0.3940	0.7460	0.5000
O6	0.190	0.894	0.095	0.191	0.894	0.095	0.192	0.896	0.095	0.1880	0.8930	0.0940
W6	0.260	0.431	0.088	0.261	0.431	0.090	0.266	0.432	0.089	0.2700	0.4340	0.0939
O7	0.766	0.860	0.093	0.769	0.862	0.093	0.778	0.868	0.093	0.7700	0.8601	0.0951
O8	0.517	0.810	0.195	0.517	0.808	0.195	0.519	0.810	0.193	0.5230	0.8110	0.1950
O9	0.989	0.047	0.199	0.988	0.046	0.199	0.986	0.046	0.199	0.9870	0.0459	0.1985
W1	0.898	0.224	0.519	0.905	0.220	0.508	0.919	0.224	0.497	0.9270	0.2190	0.5000
W2	0.362	0.233	0.507	0.379	0.240	0.506	0.378	0.238	0.502	0.3790	0.2370	0.5000
W3	0.901	0.777	0.506	0.909	0.786	0.505	0.906	0.773	0.505	0.9220	0.8000	0.5000
W1*	0.9270	0.2190	0.5160									
W3*	0.9220	0.8000	0.5160									

Note: "W" stands for the position of oxygen atom in H_2O molecules.
* Suggested positions of W1 and W3 sites based on the density profile of oxygen atoms along z-direction. The x and y coordinates are taken from data of Merlino et al. (2001). The z-coordinate corresponds to displacement 0.37 Å relative to the mirror plane in the interlayer (Fig. 7b).

performed at different temperatures, this has a negligible effect on the averaged structure of the building blocks in tobermorite (compare the results of CP2K calculations at 321 and 506 K). Table 2 does not provide the coordinates for H atoms. As we will see later, the H_2O sites in the structure of tobermorite undergo a fast rotational motion. Therefore, it is appropriate to discuss the proton distribution in terms of probability density rather then to define deterministic crystallographic sites. The reason for the differences in the experimentally determined and calculated positions of the aqueous sites and the occupancy of the W1 and W3 positions is addressed below.

The selected bond distances for the Ca and Si coordination shells are summarized in Table 3. The results obtained with the CPMD are in a good agreement with the experimental data. The simulations predict slightly shorter Ca-O distances and slightly longer Si-O bonds. Somewhat larger differences are predicted for the Ca-O6 bond. Note further that absolute agreement between calculated and experimental data cannot be expected since the size of the system and the simulation time are not sufficient to fully account for the effects of long-range disorder and possible contributions of a slow diffusive motion of the H_2O molecules in the interlayer. Additionally, the presence of minor traces of calcium ions in the interlayer, which cannot be ruled out in natural and synthetic samples of "anomalous" tobermorite, has a pronounced effect on the bond distances of the tetrahedral double chain (see Merlino et al. 2001, Table 3). An exact determination of the oxygen position in H_2O and OH groups by the experimental methods is complicated due to presence of protons, which are "invisible" to X-rays. Remarkably, the average calculated Ca-O, Ca-Si, and Ca-Ca distances are in excellent agreement with the results from EXAFS measurements (Kirkpatrick et al. 1997). In contrast to the XRD data, the EXAFS measurements probe short range order in the structure. Thus, we may expect EXAFS data to agree better with the calculations than the XRD results.

Comparing CP2K predictions with CPMD results and the experimental data, we find that the CP2K calculations systematically predict slightly longer Si-O distances. Similar behavior was noticed in the test calculations using the simple gas molecules and the solid phases. The source of this deviation lies in the accuracy of the basis set for Si atoms used in the calculations with CP2K. The accuracy could be improved by going from a double-ζ to the triple-ζ valence basis set. The larger basis set would signifi-

TABLE 3. Average interatomic distances obtained with CPMD (300 K) and CP2K (321 K) package compared to the experimental data

		CP2K	CPMD	Exp*
Ca1	O4/O4	2.325	2.325	2.368
	O8	2.325	2.315	2.356
	O3/O3	2.415	2.415	2.399
	O9	2.385	2.385	2.414
	W6	2.515	2.505	2.511
Ca3	O4	2.355	2.355	2.398
	O8/O8	2.395	2.395	2.407
	O3	2.365	2.355	2.401
	O9/O9	2.405	2.395	2.400
	O6	2.495	2.485	2.555
Si1	O1	1.685	1.665	1.649
	O2	1.675	1.645	1.637
	O3	1.635	1.615	1.599
	O4	1.625	1.605	1.609
Si2	O1	1.645	1.615	1.614
	O5	1.635	1.605	1.603
	O6	1.665	1.655	1.654
	O7	1.645	1.625	1.612
Si3	O2	1.665	1.645	1.639
	O7	1.685	1.655	1.646
	O8	1.625	1.605	1.602
	O9	1.635	1.615	1.601
		CP2K	CPMD	Exp†
Ca	O	2.39	2.38	2.42
Ca	Si	3.08	3.09	3.09
Ca	Si	3.45	3.43	3.44
Ca	Ca	3.79	3.80	3.79

Notes: The coordination shell of Ca1 sites includes two O3 and two O4 sites (two O8 and two O9 for Ca3). An average distance is given for these sites.
* X-ray diffraction data of Merlino et al. (2001).
† EXAFS data of Kirkpatrick et al. (1997).

cantly increase the computational costs, however. Therefore, it was decided to accept somewhat longer Si-O bond distances as a trade for computational costs. Note further that we could not find any artifacts related to the differences in geometries of the supercells in CPMD and CP2K calculations. Therefore, we conclude that the orthorhombic supercell used in the CP2K calculations is justified for the purpose of this study.

The vibrational density of states obtained from CPMD and CP2K trajectories are shown in Figure 2. Apart from the minor discrepancies in the absolute frequencies attributed to the artificial slow down of the light nuclei in the Car-Parrinello MD (Kuo et al. 2006), both methods show excellent agreement with the spectra shape. The form of the calculated vibrational density of states is also in good agreement with the IR absorption spectra of natural tobermorite (Garbev 2004; Yu et al. 1999). A detailed analysis of the vibrational density of states, and the interpretation of measured IR and Raman spectra, will be given in the following section.

In summary, the structural and dynamic parameters of tobermorite obtained in the simulations are in good agreement with the experimental data. The deviations between calculated and experimental structural parameters can be explained by compositional variations and structural disorder of the natural samples. The Si-O bonds obtained in CP2K simulations are slightly overestimated, but this is unlikely to have any significant effect on the structural position of the H_2O interlayer. The orthorhombic geometry of the simulations supercell is suitable for the purposes of this study.

Hydrogen bonds and orientation of H_2O molecules in the interlayer of tobermorite

OH groups in O6 sites. The unit cell of tobermorite contains four O6H groups, and two W1 and two W3 H_2O sites. The orientation of the O6H bond is determined by the geometry of long-lived O6H···W1 and O6H···W3 hydrogen bonds. According to the statistics (Table 4), each O6H group donates on average 0.5 hydrogen bond to W1 and to W3 H_2O molecules. These bonds are the shortest ones in the system and are characterized by the longest relaxation time (Table 4). In every instantaneous configuration, a half of the O6H groups in the system are bound to W1, while the other half donates hydrogen bonds to the W3 sites. During the production run at room temperature none of these bonds were broken so that every O6H group remained hydrogen bonded to one and the same W1 or W3 H_2O site. The ensemble-average angle distribution of the O6H dipoles relative to the axial orientation of the simulation cell is shown in Figure 3. The instantaneous configuration of O6H groups, which is consistent with the angular distribution, is schematically shown in Figure 4. This illustrates a "correlated" orientation of the neighboring O6H groups. Figure 4 indicates that the O6H dipoles are oriented out of the (010) plane, and therefore the "instantaneous" configurations violate the layer group symmetry $C2m(m)$. Such an orientation of the O6H groups is the consequence of a strong electrostatic repulsion between neighboring O6H protons. By contrast, the orientation of the OH groups in the next neighboring layer is random, so that the group symmetry of the building block, $C2m(m)$, is retained as an ensemble average. Although the flipping of hydrogen bonds between O6H···W1 and O6H···W3 had not been observed during the production time at room temperature (likely due to the small size of the system and the rather short simulation time ~20 ps) such transformations may occur in the natural samples on the longer time scale or higher temperatures. To promote the reorientation dynamics of hydrogen bonds, an additional run at 506 K was performed.

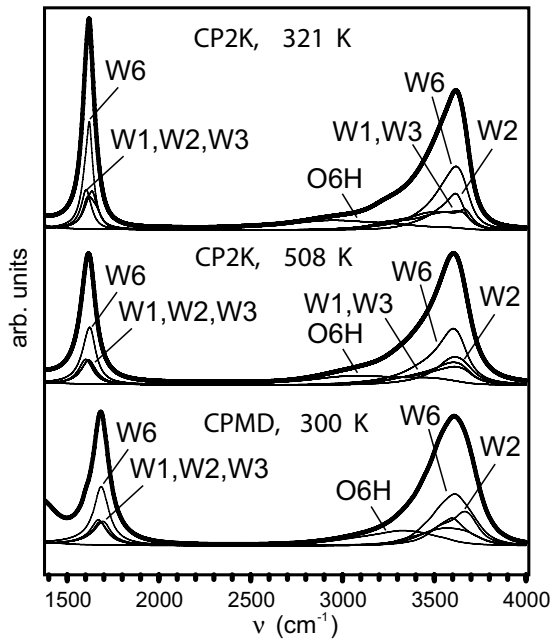

FIGURE 2. Total vibrational density of states (thick line) and the individual contributions from H atoms associated with O6, W6, W1, W2, and W3 sites (thin lines) obtained from CPMD and CP2K simulations. The frequencies of CPMD results are scaled by $1.04\cdot\sqrt{2}$ to correct for isotopic substitution and the fictitious dynamics of electrons.

TABLE 4. Position of the first maximum R_{max} of the hydrogen-oxygen radial distribution function, average number of hydrogen bonds n_{HB}, and hydrogen-bonds relaxation time $\tilde{\tau}_{ij}$ (Eq. 2)

	CP2K (321 K)			CP2K (506 K)		
	$R_{max,1}$ (Å)	n_{HB}	$\tilde{\tau}_{ij}$ (ps)	$R_{max,1}$ (Å)	n_{HB}	$\tilde{\tau}_{ij}$ (ps)
O6H···W1	1.59/1.63	0.50	>20	1.65	0.49	1.35
O6H···W3	1.57/1.63	0.50	>20	1.63	0.45	1.57
W6H···W2	1.91	0.29	0.3	1.87	0.28	0.21
W6H···W3	2.01	0.18	0.17	1.93	0.17	0.17
W6H···W1	2.00	0.15	0.17	1.90	0.14	0.15
W6H···O7	2.02	0.17	0.17	1.98	0.16	0.11
W6H···O1	2.03	0.15	0.17	2.03	0.15	0.10
W6H···O2	–	0.13	0.08	–	0.12	0.06
W1H···W2	1.79	0.24	1.36	1.82	0.23	0.29
W1H···W6	1.73	0.37	0.58	1.87	0.28	0.19
W1H···O1	1.79	0.34	0.18	1.81	0.41	0.14
W1H···O6	1.99	0.09	0.18	–	0.9	0.08
W2H···O2	1.89	0.45	0.7	1.96	0.4	0.14
W2H···O7	2.02	0.30	0.33	–	0.24	*
W2H···O1	2.01	0.31	0.33	–	0.26	0.11
W2H···W6	2.12	0.13	0.12	–	0.14	0.10
WH3···W2	1.77	0.25	0.79	1.77	0.23	0.21
WH3···W6	1.75	0.32	*	1.79	0.26	0.21
WH3···O7	1.85	0.35	0.2	1.89	0.40	0.14
WH3···O6	2.11	0.12	0.2	–	0.10	0.13

Note: Dash = Maximum cannot be clearly identified.
* Decay cannot be described with a single exponent.

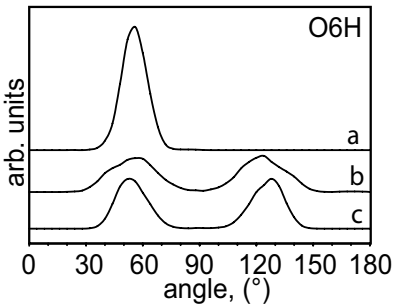

FIGURE 3. Time-ensemble averaged distribution of the angle formed between the O6H bond and the **a**, **b**, and **c** directions in the simulation supercell obtained from CP2K trajectory at 321 K.

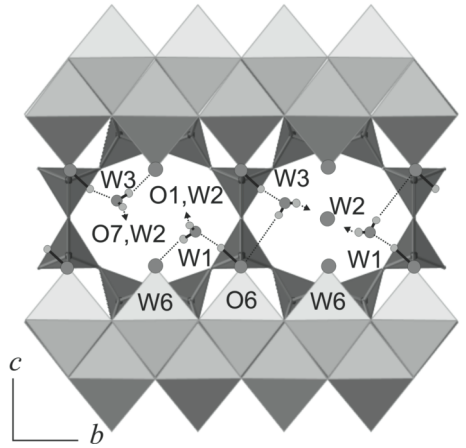

FIGURE 4. Schematic view of an instantaneous arrangement of the OH groups forming strong H bonds with the W1 and W3 sites. Possible hydrogen bonds donated by W1 and W3 sites are also indicated (W1: O6···HOH···W2, W6···HOH···W2, W6···HOH···O1; W3: O6···HOH···W2, W6···HOH···W2, W6···HOH···O7).

At this temperature the kinetic energy was sufficient for transformations between O6H···W1 and O6H···W3 configurations within the simulation time of 20 ps (see the following section). The time-dependent variation of O6H···W1 and O6H···W3 bond distances $\Delta R_{HB}(t)$ for two arbitrary O6H groups together with the bond formation function $h(t)$ is shown in Figure 5. The latter parameters are defined as follows:

$$\Delta R_{HB}(t) = R(\text{O6H}\cdots\text{W1}, t) - R(\text{O6H}\cdots\text{W3}, t) \quad (4)$$

$$h(t) = \begin{cases} 1, & \text{if } \Delta R_{HB}(t) \geq 0 \\ -1, & \text{if } \Delta R_{HB}(t) < 0 \end{cases} \quad (5)$$

The evolution of $\Delta R_{HB}(t)$ clearly indicates that O6H···W1 to O6H···W3 transformations take place at 506 K. A similar behavior of OH groups was detected by ab initio simulations and NMR measurements in the structure of OH-topaz (Churakov and Wunder 2004; Xue et al. 2006).

W1 and W3 H_2O sites. The structural orientation of the H_2O molecules in the W1 and W3 sites was found to have remarkable similarities. The position of oxygen atoms in the W1 and W3 sites is controlled by the long-lived hydrogen bonds with the O6H groups (Table 4; see also the section on O6H sites).

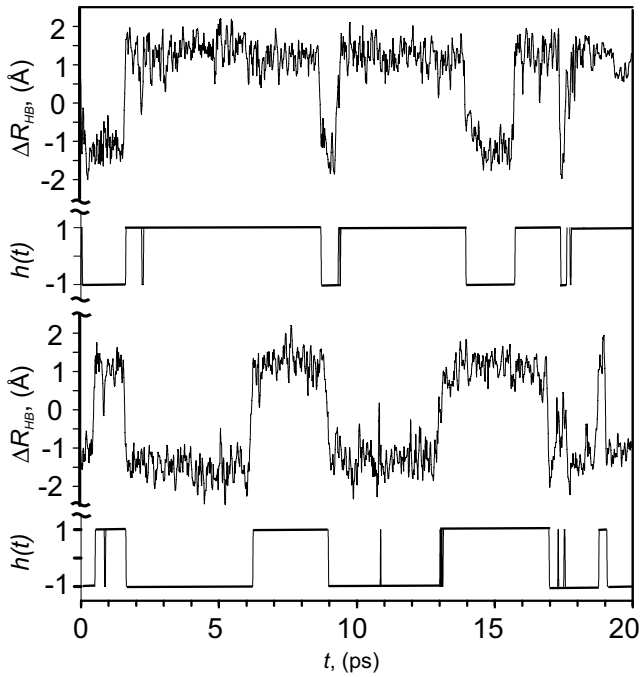

FIGURE 5. Time evolution of the difference between hydrogen bond distances $\Delta R_{HB}(t)$ (Eq. 4) and bond formation function $h(t)$ (Eq. 5) shown for two different O6H groups at 506 K.

Density profiles of O atoms along the *c* direction indicate that the averaged coordinates of the W1 and W3 sites are split into two sub-positions with 0.5 occupancy, shifted relative to the (001) mirror plane by 0.37 Å (Fig. 6). The occupancy of split O sites depends on the hydrogen bonds formed by H_2O molecules with the "upper" or "lower" O6H groups (with respect to the *c* axis). Since the transformation of O6H···W1 to O6H···W3 could not be observed at room temperature, the W1 and W3 sites occupy one and the same "upper" (or "lower") sites during the entire simulation time, as is shown in Figure 6. At 506 K, the kinetic energy of molecules was sufficient to break the O6H···W1 and O6H···W3 bonds (Fig. 5). As a consequence, the W1 and W3 H_2O molecules were able to jump between "upper" and "lower" sites. The density profiles of W1 and W3 sites at 321 and 506 K are compared in Figure 7a. The distribution for 506 K has not fully converged to the equilibrium profile and the influence of the initial configuration of H_2O sites is obvious. However, the transition of the molecules between neighboring sites can be clearly seen. If we take into account the independent dynamics of the W1 and W3 sites in the next neighboring interlayer, the ensemble averaged distribution at 321 K resulted in a "double hill" profile (Fig. 7b). Such a break up of the W1 and W3 sites observed in the simulations could explain the unusually large displacement factor reported in XRD studies for these sites (Merlino et al. 1999, 2001).

The statistics of various hydrogen bonds donated by the W1 and W3 sites is given in Table 5. The preferential orientation of these sites is shown schematically in Figures 4, 8c, and 8d. The W1H···W2 and W3H···W2 are the bonds with the longest relaxation time for the W1 and W3 sites. Therefore, these bonds control the orientation and position of W2 molecules (see below). Considering a local (instantaneous) symmetry,

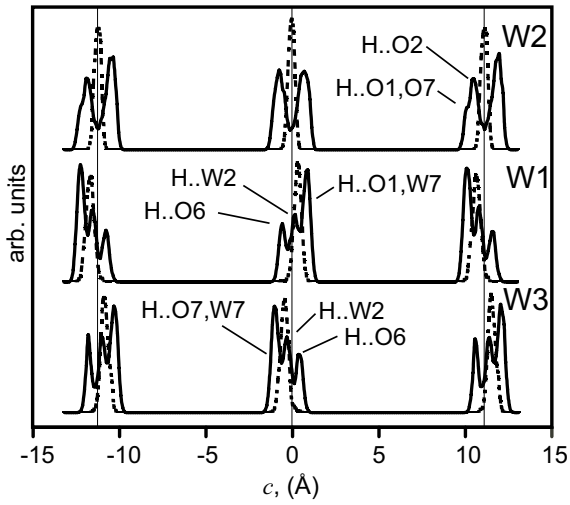

FIGURE 6. Average atomic density profile of O (dashed lines) and H (solid lines) atoms along the **c** direction of the simulation cell for W1, W2, and W3 sites at 321 K. Note that the obtained distributions for W1 and W3 sites violate the mirror plane (thin vertical line) in the tobermorite structure suggested by X-ray measurements (Merlino et al. 2001).

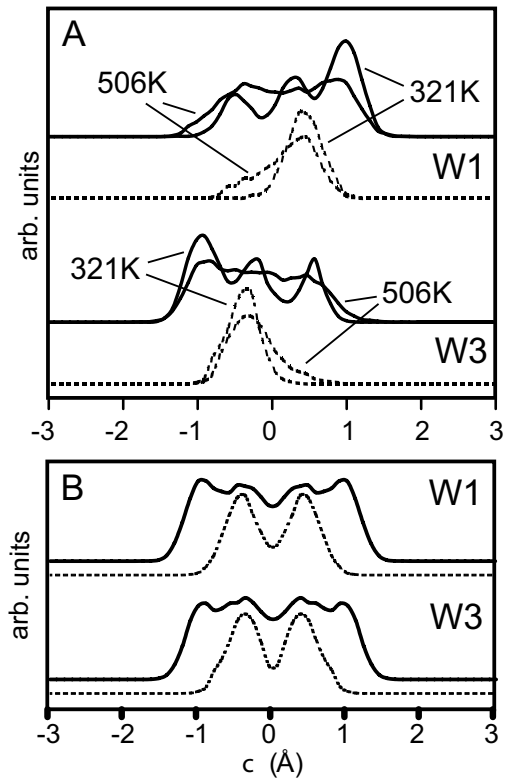

FIGURE 7. (**a**) Density profiles for O (dotted line) and H (solid) atoms in a single interlayer for the W1 and W3 sites obtained from CP2K trajectory at 321 and 506 K. (**b**) Density profiles for 321 K trajectory averaged over neighboring interlayer and the mirror plane as suggested by X-ray refinement by Merlino et al. (2001). The distribution of O sites clearly indicates the splitting of O positions relative to the mirror plane. The symmetry averaged profiles of O atoms in W1 and W3 sites are identical. The small differences in the density profiles of H atoms in W1 and W3 sites could be attributed to deficient statistics due to the short simulation time (~20 ps), rather then the structural differences.

the O1···HW1H···W6 and W6···HW3H···O7 hydrogen-bond chains are structurally equivalent. Other relevant configurations (Table 5) are W2···HW1H···O1, W2···HW1H···O6, and W2···HW1H···W6, which correspond to W2···HW3H···O7, W2···HW3H···O6, and W2···HW1H···W6.

W2 sites H_2O sites. The orientation of the W2 sites (Fig. 8a) can be explained based on the hydrogen-bond connectivity (Table 5), the distribution of the H_2O dipole moments (not shown), and the density profile of O and H atoms. The O atom of the W2 site is situated on the mirror plane in the center of the interlayer (Fig. 5). The plane of the H_2O molecule is oriented sub-parallel to the (100) crystal plane with the dipole moment pointing along the "*a*" direction. Such an orientation of the dipole moment is predetermined by the chain of hydrogen bonds O6H···W1H···W2 or O6H···W3H···W2 (Fig. 8d). For every instantaneous configuration of W2 sites, one H atom donates a hydrogen bond to the O2 atom, while the second OH contact forms a hydrogen bond to the O7 or O1 atom from the opposite (with respect to the "*a*-*b*" plane) tetrahedral chain with a 50% probability. By considering fast reorientation dynamics of the W2 sites, the following types of motion are expected: transition between O2···HW2H···O7 to O2···HW2H···O1, from O2···HW2H···O7 to O7···HW2H···O2, and from O2···HW2H···O1 to O1···HW2H···O7. The average lifetime of these hydrogen bonds is substantially below the average life-time of hydrogen bonds in bulk H_2O at ambient conditions (Table 4).

W6 H_2O sites. The W6 sites have the characteristics of strongly absorbed H_2O molecules on the surface of the Ca layer. The lone electron pair points to the Ca1 sites. The W6H···W2 is the strongest and statistically dominant hydrogen bond, which mainly constrains the orientation of the W6 site (Tables 4 and 5). Weaker hydrogen bonds are donated to W1, W3, O1, O7, and O2 sites (Table 5). Figure 8b schematically illustrates the preferential orientations of W6 H_2O molecules. The reorienta-

TABLE 5. Probability (in percents) of H_2O configurations with a particular connectivity of hydrogen bonds (O_x···HW_nH···O_y), obtained from CP2K trajectory at 321 K

HW6H	···O1	···O2	···O7	···W1	···W2	···W3
O1···	0					
O2···	2	0				
O7···	1	2	0			
W1···	1	6	4	0		
W2···	13	0	18	11	0	
W3···	7	7	1	6	12	0
HW2H	···O1	···O2	···W6	···O7		
O1···	3					
O2···	31	2				
W6···	10	1	0			
O7···	2	29	11	3		
HW1H	···O1	···O6	···W6	···W2		
O1···	2					
O6···	1	0				
W6···	43	0	5			
W2···	11	18	19	0		
HW3H	···O6	···W6	···O7	···W2		
O6···	0					
W6···	0	2				
O7···	2	42	1			
W2···	23	15	10	0		

Notes: The O_x and O_y are the names of oxygen sites given in the row and column, respectively, for W6, W2, W1, and W3 H_2O sites. The results for 506 K (not shown) are essentially similar.

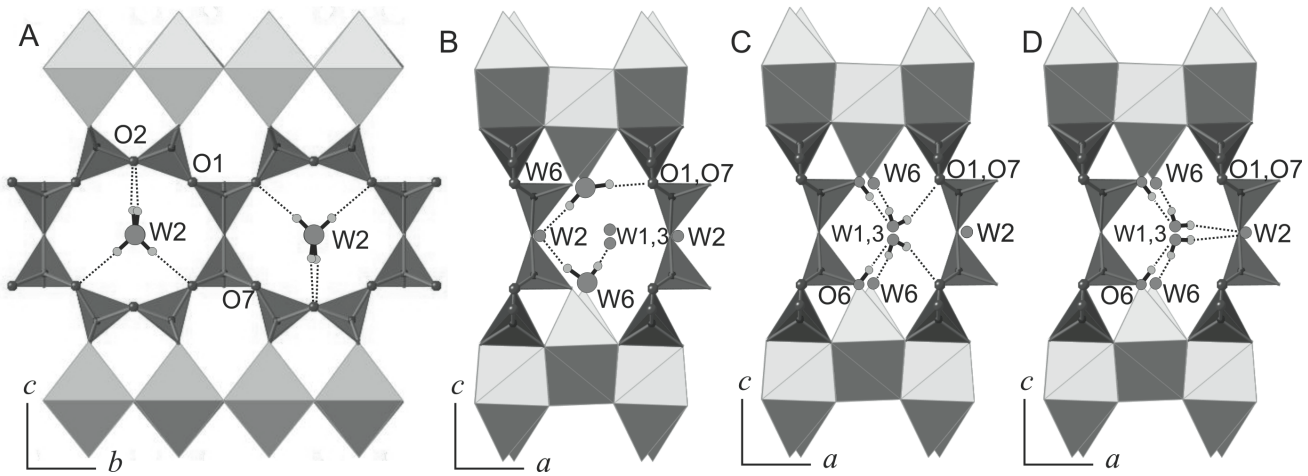

FIGURE 8. Preferential orientations of hydrogen bonds formed by interlayer H_2O in the tobermorite structure (schematic). In the (*ac*) projection, the positions of W1 and W3 sites almost coincide. (**A**) Four possible orientation of W2 H_2O molecules (O2···HOH···O1 and O2···HOH···O7). (**B**) Orientation of W6 sites (W2···HOH···O1, W2···HOH···O7, W2···HOH···W1, and W2···HOH···W3) (**C**, **D**) Orientation of O6H, W1, and W3 sites (W1: O1···HOH···W6, O1···HOH···W2, and W2···HOH···W6; W3: O7···HOH···W6, O7···HOH···W2, and W2···HOH···W6).

tion dynamics of W6 sites include the transformations between W2···HW6H···O1,O7 and W2···HW6H···W1,W3 hydrogen bonded configurations.

Vibrational density of states

Figure 2 represents the vibrational density of states obtained from CPMD and CP2K calculations in the 1500–4000 cm^{-1} frequency range. Apart from the minor discrepancies in the absolute frequencies, both methods provide a remarkably similar shape for the vibration spectra. The asymmetric peak with a maximum at 3630 cm^{-1}, and two broad shoulders at 3300 and 3000 cm^{-1}, represent the stretching modes of OH groups. The sharp band at 1620 cm^{-1} is related to bending modes of H_2O molecules. The total spectrum is resolved into individual contributions from different H_2O sites and O6H groups. The W1, W2, W3, and W6 sites provide the main contributions to the 3630 cm^{-1} band as well as a smaller contribution to the 3300 cm^{-1} band. The O6H sites are entirely responsible for shoulder at 3000 cm^{-1} and also provide a smaller contribution to the band at 3300 cm^{-1}. Note that the O6H group does not contribute to the H_2O bending band at 1620 cm^{-1}. Half of the intensity of the W6 band almost exactly coincides with the contribution due to the W2 site (there are two times more W6 molecules than W2 molecules in the unit cell), indicating that both sites have a similar environment in terms of hydrogen bond strength. The shape of the W1 and W3 contributions are almost identical thus supporting the idea of the similar structural role of these sites, as suggested by the analysis of the hydrogen bond connectivity.

Both the high- (506 K) and low- (321 K) temperature spectra are very similar. A minor temperature effect is indicated in the "smoothness" of the W1 and W3 bands due to the larger translational freedom of the molecules at higher temperatures. From a comparison of CP2K and CPMD data, one can infer that the 3300 cm^{-1} band in the O6H contribution obtained with CPMD is stronger than that obtained with CP2K. We believe that the CP2K simulations are superior to CPMD results since the Car-Parrinello approach is known to have a strong dependence on the choice of the fictitious electron mass. Additionally, the present CPMD results have a lower statistical significance due to the shorter simulation time.

DISCUSSION

Static and dynamic disorder in the structure of anomalous tobermorite

The experimental studies describe an order-disorder character of the tobermorite phases associated with the relative arrangement of the building blocks and the distribution of the Ca ions in the interlayer (Merlino et al. 1999, 2001). The present results reveal a new level of structural heterogeneities in anomalous tobermorite associated with the dynamics of H_2O molecules in the interlayer. The following types of order-disorder related to hydrogen bonding have been identified: (1) orientational order-disorder of O6H groups in the interlayer, associated with the long-lived O6H···W1 and O6H···W3 hydrogen bonds and partial occupation of W1 and W3 sites, and (2) short-time disorder associated with fast reorientation dynamics of donation hydrogen bonds formed by W1, W3, W2, and W6 H_2O molecules.

The results of MD simulations strongly suggest that the W1 and W3 sites are located in general positions with 50% residence time at coordinates (0.927, 0.219, 0.516) and (0.922, 0.800, 0.516), respectively, in contrast to the special positions (0.927, 0.219, 0.500) and (0.922, 0.800, 0.500) with 100% occupancy reported from XRD studies (Merlino et al. 1999, 2001). The reported experimental sites correspond to an average of the split positions obtained in the simulations. The unusually high displacement factors reported for W1 and W3 sites in XRD studies (see Table 2 in Merlino et al. 2001) further support our conclusion concerning the split in W1 and W3 sites (Fig. 7b). Based on the findings from this study the XRD measurements could be reinterpreted to obtain more precise coordinates of the W1 and W3 sites.

No transition of W1 and W3 molecules between neighboring sites was observed during 20 ps molecular dynamic trajectory at 321 K. In contrast, at 506 K such transitions occur within a short simulation run. This observation indicates the possibility

of a temperature-induced order-disorder phase transition in anomalous tobermorite in the temperature interval 300–500 K associated with the orientation-ordering of O6H dipoles and the H_2O distribution in the W1 and W3 sites. In principle, such a phase transition could be detected with the help of NMR spectroscopy. Therefore, we encourage the experimental community to investigate such a phenomenon.

Interpretation of IR and Raman spectra

The vibrational density of states calculated for tobermorite can be compared with the experimental IR and Raman studies on natural and synthetic samples. The intensity of IR spectra is related to the dynamic variation of the dipole moment of the system (Silvestrelli et al. 1997). The intensity of Raman spectra depends on dynamic variations of the polarizability tensor (Putrino and Parrinello 2002). Since the dipole moment and the polarizability depend on both atomic positions and the distribution of electron density, the amplitude of vibrational density of states is not identical to the IR or Raman spectra. Nevertheless, the positions of the vibrational frequencies are interrelated. IR absorption spectra of natural and synthetic 11 Å tobermorite were reported by Yu et al. (1999) and Garbev (2004). The C/S ratio of the 11 Å tobermorite studied by Yu et al. (1999) was 0.8, which indicates the presence of significant amounts of Ca in the interlayer. The experimental studies report an asymmetric IR absorption band with a maximum at 3600 cm^{-1}, and a weak shoulder at 3300 cm^{-1}. These bands are in excellent agreement with the calculated vibrational density of states (Fig. 2). In contrast to the calculations, there are no unambiguous indications for absorption at 3000 cm^{-1} in the measured spectra, for the following reasons: the calculated 3000 cm^{-1} band attributed to O6H stretching is very weak and can only be clearly resolved by analyzing individual contributions from the different H sites. The experimentally investigated 11 Å tobermorites have a high content of interlayer Ca ions. From the structure of normal tobermorite it is known that the concentration of O6H groups is anti-correlated with the concentration of Ca in the interlayer. Therefore, we believe that the weak band at 3000 cm^{-1} band is simply hidden in the background. Additionally, the experimental spectra are "contaminated" by contributions from the H_2O molecules bonded to interlayer Ca ions. Thus, detailed simulations of "normal" 11 Å tobermorite that include order-disorder phenomena will be necessary to completely resolve the nature of experimental IR and Raman spectra of 11 Å tobermorite.

A possible hint as to the nature of the vibration bands at 3000 cm^{-1} can be gained from the rather controversially discussed phase, referred as 10 Å tobermorite. Formation of this phase was observed by Bonaccorsi and Merlino (2000) after heating anomalous tobermorite at 773 K. Another synthesis route for this phase might be the mixed hydrothermal product of gyrolite and 10 Å tobermorite obtained from amorphous CaO and SiO_2 at 453–483 K (Garbev 2004; Jauberthie et al. 1996). It is not clear, however, if these phases are all identical. The C/S ratio in the 10 Å tobermorite is similar to the one in the "anomalous" 11 Å polymorph, but the H_2O content is lower. The Raman spectrum of hydrothermally synthesized 10 Å tobermorite was reported by Garbev (2004). The spectrum contains two weak bands at 3648 and 3490 cm^{-1}, and a very strong double band at 2938 and 2869 cm^{-1}. On the assumption that the 10 Å polymorph merely represents strongly dehydrated anomalous 11 Å tobermorite, one could argue that the traces of H_2O available in the 10 Å polymorph are the W1,W3-like H_2O molecules. As a consequence, the hydrogen bonded to the O6H groups, would be responsible for the bands at 2938 and 2869 cm^{-1}. Note, however, that the proposed interpretation is very speculative, since 10 Å tobermorite is very poorly characterized.

Water diffusion in tobermorite

An important aspect of tobermorite chemistry is the ability of water molecules and ions to diffuse in the interlayer of tobermorite and C-S-H phases. The simulation time of 20 ps was not sufficient to observe the diffusive process even at 506 K. It should be noted that water diffusion in idealized anomalous tobermorite may be different from that in natural samples. On the one hand, the natural samples contain interlayer ions that are likely to slow down the water diffusion by fixing the water molecules to their hydration shell. On the other hand, defects in the structure and partial occupation of the available water sites due to compositional variations can substantially facilitate diffusion. It was recently shown, in the case of xonotlite, that defects in the tetrahedral double chain are likely to occur in pairs (Churakov and Mandaliev 2007). Similar types of defects in the bridging tetrahedra of tobermorite would open additional possibilities for the diffusion of water molecules and ions. To the best of our knowledge direct measurements or simulations of water diffusion in tobermorite crystalline phases are not available. A good estimate may be obtained from simulations of the tobermorite-water interface and water diffusion measurements in C-S-H phases. Classical MD simulations of the water-tobermorite interface revealed the existence of "slowly" diffusing near-surface water molecules (Kalinichev et al. 2007). The diffusion coefficient of surface H_2O can be considered as an upper limit for interlayer diffusion of water in tobermorite. The simulation and the experimental data predict diffusion coefficients for surface H_2O as low as 5×10^{-11} and 6×10^{-10} m^2/s for "strongly" and "weakly" bonded molecules respectively (Korb et al. 2007). Note that a simulation trajectory as long as at least ~10 ns would be necessary to estimate such a slow process. This is far beyond the performance of ab initio methods on the presently existing computational resources. Therefore, it is challenging to develop a classical force field capable of reproducing the structural and dynamical properties of the crystalline and amorphous C-S-H phases, which will allow the atomistic simulations of transport phenomena in cement to be carried out.

ACKNOWLEDGMENTS

The simulations have been performed on the CRAY-XT3 in the CSCS. The author is grateful to Marcella Iannuzzi and Mathias Krack for assistance in setting up the CP2K simulations. I thank Peter Mandaliev, Erich Wieland, Daniele Passerone, and Thomas Armbruster for fruitful discussions of the results. Partial financial support was provided by the National Cooperative for the Disposal of Radioactive Waste (Nagra), Switzerland.

REFERENCES CITED

Allen, M.P. and Tildesley, D.J. (1987) Computer Simulations of Liquids, 386 p. Clarendon Press, Oxford.

Becke, A.D. (1988) Density-functional exchange-energy approximation with correct asymptotic behavior. Physical Review A, 38, 3098–3100.

Bell, I.S. and Coveney, P.V. (1998) Molecular modeling of the mechanism of ac-

tion of borate retarders on hydrating cements at high temperature. Molecular Simulations, 20, 331–356.
Blöchl, P.E. and Parrinello, M. (1992) Adiabaticity in first-principles molecular dynamics. Physical Review B, 45, 9413–9416.
Bonaccorsi, E. and Merlino, S. (2000) Crystal chemistry and structure arrangements of "normal" and "anomalous" tobermorite 11 Å. Proceedings of the Sixth International Congress on Applied Mineralogy, 2, 335–338.
Bonaccorsi, E., Merlino, S., and Kampf, A.R. (2005) The crystal structure of tobermorite 14 Å (Plombierite), a C-S-H phase. Journal of the American Ceramic Society, 88, 505–512.
Car, R. and Parrinello, M. (1985) Unified approach for molecular dynamics and density-functional theory. Physical Review Letters, 55(22), 2471–2474.
Chandler, D. (1987) Introduction to the Modern Statistical Mechanics, 242 p. Oxford University Press, New York.
Churakov, S.V. and Mandaliev, P. (2007) Structure of the hydrogen bonds and silica defects in the tetrahedral double chain of xonotlite. Cement and Concrete Research, 38, 300–311.
Churakov, S.V. and Wunder, B. (2004) Ab-initio calculations of the proton location in topaz-OH, $Al_2SiO_4(OH)_2$. Physics and Chemistry of Minerals, 31, 131–141.
Cong, X.D. and Kirkpatrick, R.J. (1996) Si-29 and O-17 NMR investigation of the structure of some crystalline calcium silicate hydrates. Advanced Cement Based Materials, 3, 133–143.
Coveney, P. and Humphries, W. (1996) Molecular modeling of the mechanism of action of phosphonate retarders on hydrating cements. Journal of the Chemical Society, 92, 831–841.
CPMD (1997–2001) Car-Parrinello Molecular Dynamics (CPMD) v.3.9. Copyright IBM Corp. 1990–2008, Copyright MPI für Festkoerperforschung Stuttgart, 1997–2001.
Faucon, P., Delaye, J.M., Virlet, J., Jacquinot, J.F., and Adenotg, F. (1997) Study of the structural properties of the C-S-H(I) by molecular dynamic simulations. Cement and Concrete Research, 27, 1581–1590.
Faucon, P., Delagrave, A., Petit, J.C., Richet, C., Marchand, J.M., and Zanni, H. (1999) Aluminum incorporation in calcium silicate hydrates (C-S-H) depending on their Ca/Si ratio. Journal of Physical Chemistry B, 103, 7796–7802.
Garbev, K. (2004) Structure properties and quantitative Rietveld analysis of calcium silicate hydrates crystallized under hydrothermal conditions, p. 271. Ph.D. thesis, Forschungs Zentrum Karlsruhe, Karlsruhe.
Gmira, A., Zabat, M., Pellenq, R.J.M., and van Damme, H. (2004) Microscopic physical basis of the poromechanical behavior of cement-based materials. Materials and Structures, 37, 3–14.
Goedecker, S. (1999) Linear scaling electronic structure methods. Review of Modern Physics, 71, 1085–1123.
Goedecker, S., Teter, M., and Hutter, J. (1996) Separable dual-space Gaussian pseudopotentials. Physical Review B, 54, 1703–1710.
Grossman, J.C., Schwegler, E., Draeger, E.W., Gygi, F., and Galli, G. (2004) Toward assessment of the accuracy of density functional theory for first principle simulations of water. Journal of Chemical Physics, 120, 300–311.
Hohenberg, P. and Kohn, W. (1964) Inhomogeneous electron gas. Physical Review, 136, 864–871.
Hoover, W.G. (1985) Canonical dynamics: Equilibrium phase-space distributions. Physical Review A, 31, 1695–1697.
Jantzen, C.M. (1984) Radioctive waste-portland-cement systems: II, Leaching characteristics. Journal of the American Ceramic Society, 67, 674–678.
Jauberthie, R., Temimi, M., and Laquerbe, M. (1996) Hydrothermal transformation of tobermorite gel to 10 Å tobermorite. Cement and Concrete Research, 26, 1335–1339.
Kalinichev, A.G. and Churakov, S.V. (2001) Thermodynamics and structure of molecular clusters in supercritical water. Fluid Phase Equilibria, 183–184, 271–278.
Kalinichev, A.G. and Kirkpatrick, R.J. (2002) Molecular dynamics modeling of chloride binding to the surfaces of calcium hydroxide, hydrated calcium aluminate, and calcium silicate phases. Chemistry of Materials, 14, 3539–3549.
Kalinichev, A.G., Wang, J., and Kirkpatrick, R.J. (2007) Molecular dynamics modeling of the structure, dynamics and energetics of mineral-water interfaces: Application to cement materials. Cement and Concrete Research, 37, 337–347.
Kashihara, S., Yamanaka, S., Inoue, T., Komatsu, T., and Toyoshima, H. (1994) Quantum-chemical determination of the Al-substituted site in tobermorite. Journal of the American Ceramic Society, 77, 3023–3026.
Kirkpatrick, R.J., Brown, G.E., Xu, N., and Cong, X.D. (1997) Ca X-ray absorption spectroscopy of C-S-H and some model compounds. Advances In Cement Research, 9, 31–36.
Kirkpatrick, R.J., Kalinichev, A.G., Hou, X., and Struble, L. (2005) Experimental and molecular dynamics modeling studies of interlayer swelling: water incorporation in kanemite and ASR gel. Materials and Structures, 38, 449–458.
Kohn, W. and Sham, L.J. (1965) Self-consistent equation including exchange and correlation effects. Physical Review, 140(4A), A1133–A1138.
Korb, J.-P., McDonald, P.J., Monteilhet, L., Kalinichev, A.G., and Kirkpatrick, R.J. (2007) Comparison of proton field-cycling relaxometry and molecular dynamics simulations for proton-water surface dynamics in cement-based materials. Cement and Concrete Research, 37, 348–350.
Kuo, I.-F.W., Mundy, C.J., McGrath, M.J., Siepmann, J.I., VandeVondele, J., Sprik, M., Hutter, J., Chen, B., Klein, M.L., Mohamed, F., Krack, M., and Parrinello, M. (2004) Liquid water from first principles: investigation of different sampling approaches. Journal of Physical Chemistry B, 108, 12990–12998.
Kuo, I.-F.W., Mundy, C.J., McGrath, M.J., and Siepmann, J.I. (2006) Time-dependent properties of liquid water: A comparison of Car-Parrinello and Born-Oppenheimer molecular dynamics simulations. Journal of Chemical Theory and Computation, 2, 1274–1281.
Lee, C., Yang, W., and Parr, R.G. (1988) Development of the Colle-Salvetti correlation-energy formula into a functional of the electron density. Physical Review B, 37, 785–789.
Lippert, G., Hutter, J., and Parrinello, M. (1997) A hybrid Gaussian and plane wave density functional scheme. Molecular Physics, 92, 477–488.
Megaw, H.D. and Kelsey, C.H. (1956) Crystal structure of tobermorite. Nature, 177, 390–391.
Merlino, S., Bonaccorsi, E., and Armbruster, T. (1999) Tobermorites: Their real structure and order-disorder (OD) character. American Mineralogist, 84, 1613–1621.
——— (2001) The real structure of tobermorite 11 Å: Normal and anomalous forms, OD character and polytypic modifications. European Journal of Mineralogy, 13, 577–590.
Nose, S. (1984) A molecular dynamics method for simulations in the canonical ensemble. Molecular Physics, 52, 255–268.
Payne, M.C., Teter, M.P., Allan, D.C., Arias, T.A., and Joannopoulos, J.D. (1992) Iterative minimization techniques for ab initio total-energy calculations: Molecular dynamics and conjugate gradients. Review of Modern Physics, 64, 1045–1097.
Perdew, J.P., Burke, K., and Ernzerhof, M. (1996) Generalized gradient approximation made simple. Physical Review Letters, 77, 3865–3868.
Press, W., Flannery, H., Teukolsky, B.P., and Vetterling, W.T. (1992) Numerical recipes in FORTRAN 77: The art of scientific computing. Cambridge University Press, U.K.
Putrino, A. and Parrinello, M. (2002) Anharmonic Raman spectra in high-pressure ice from ab initio simulations. Physical Review Letters, 88, 176401–176405.
Rapaport, D.C. (1983) Hydrogen bonds in water. Network organization and lifetimes. Molecular Physics, 50, 1151–1162.
Richardson, I.G. (2004) Tobermorite/jennite- and tobermorite/calcium hydroxide-based models for the structure of C-S-H: Applicability to hardened pastes of tricalcium silicate, β-dicalcium silicate, Portland cement, and blends of Portland cement with blast-fumace slag, metakaolin, or silica fume. Cement and Concrete Research, 34, 1733–1777.
Schwegler, E., Grossman, J.C., Gygi, F., and Galli, G. (2004) Towards an assessment of the accuracy of density functional theory for first principles simulations of water. II. Journal of Chemical Physics, 121, 5400–5409.
Silvestrelli, P.L., Bernasconi, M., and Parrinello, M. (1997) Ab initio infrared spectrum of liquid water. Chemical Physics Letters, 277, 478–482.
Tangney, P. (2006) On the theory underlying the Car-Parrinello method and the role of the fictitious mass parameter. Journal of Chemical Physics, 124, 044111.
Tangney, P. and Scandolo, S. (2002) How well do Car-Parrinello simulations reproduce the Born-Oppenheimer surface? Theory and examples. Journal of Chemical Physics, 116, 14–24.
Taylor, H.F.W. (1997) Cement Chemistry, 457 p. Thomas Telford Publishing, London.
Troullier, N. and Martins, J.L. (1991) Efficient pseudopotentials for plane-wave calculations. Physical Review B, 43, 1993–2006.
VandeVondele, J., Krack, M., Mohamed, F., Parrinello, M., Chassaing, T., and Hutter, J. (2005) Quickstep: Fast and accurate density functional calculations using a mixed Gaussian and plane waves approach. Computer Physics Communications, 167, 103–128.
Wieker, W., Grimmer, A.R., Winkler, A., Mägi, M., Tarmak, M., and Lippmaa, E. (1982) Solid-state high-resolution ^{29}Si NMR spectroscopy of synthetic 14, 11, and 9 Å tobermorites. Cement and Concrete Research, 12, 333–339.
Xue, X., Kanzaki, M., Fukui, H., Ito, E., and Hashimoto, T. (2006) Cation order and hydrogen bonding of high-pressure phases in the Al_2O_3-SiO_2-H_2O system: An NMR and Raman study. American Mineralogist, 91, 850–861.
Yu, P., Kirkpatrick, R.J., Poe, B., McMillan, P.F., and Cong, X.D. (1999) Structure of calcium silicate hydrate (C-S-H): Near-, mid-, and far-infrared spectroscopy. Journal of the American Ceramic Society, 82, 742–748.

MANUSCRIPT RECEIVED DECEMBER 21, 2007
MANUSCRIPT ACCEPTED AUGUST 4, 2008
MANUSCRIPT HANDLED BY BARRY BICKMORE